INDIAN JOURNAL OF SCIENCE AND TECHNOLOGY

RESEARCH ARTICLE

Psychological Driver Sensitivity in Lattice Hydrodynamic Traffic Model under Passing Behaviour

Meenakshi Mehra[1], Sunita Yadav[1], Poonam Redhu[1]*

1 Department of Mathematics, Maharshi Dayanand University, Rohtak, 124001, Haryana, India

OPEN ACCESS

Received: 25-01-2024

Accepted: 06-03-2024

Published: 02-07-2024

Citation: Mehra M, Yadav S, Redhu P (2024) Psychological Driver Sensitivity in Lattice Hydrodynamic Traffic Model under Passing Behaviour. Indian Journal of Science and Technology 17(26): 2708-2718. https://doi.org/10.17485/IJST/v17i26.208

* **Corresponding author**.

Poonamr.maths@mdurohtak.ac.in

Funding: None

Competing Interests: None

Published By Indian Society for Education and Environment (iSee)

ISSN
Print: 0974-6846
Electronic: 0974-5645

Abstract

Objectives: In order to control and manage the traffic flow in contexts of congestion, real-time highway traffic flow models play a significant role in intelligent transportation system. The objective of our investigation is to examine the effect of psychological driver sensitivity (PDS) when coupled with passing behaviour. **Methods:** In this study, we developed the lattice hydrodynamic (LH) model which is a good and simple representation for solving traffic problems. Its variants have been valuable tools in traffic research and also contributed to our understanding of traffic phenomena and the development of traffic management strategies. The effect of the proposed LH model with the factor PDS and passing is examined through linear stability analysis. Employing nonlinear stability analysis, we are able to establish the permissible range of PDS values in conjunction with a passing constant, ensuring the existence of kink soliton solution for the mKdV equation. **Findings:** To validate our theoretical findings, we conducted numerical simulation, conclusively demonstrating that the integration of PDS with passing in the proposed model, can efficiently mitigate traffic congestion. When we fix the passing coefficient and vary the PDS coefficient, we identify the enlargement of stable region with small PDS values. Similarly, by fixing the PDS coefficient varying passing coefficient reveals the enlargement of stable region with small passing values. **Novelty:** Results displayed that the stability performance of the proposed model is higher than the existing LH model with passing and found that our proposed model performs better than existing models to alleviate traffic congestion and improve traffic flow.

Keywords: Traffic flow; Lattice hydrodynamic model (LHM); Psychological driver sensitivity (PDS); Passing effect; Stability

1 Introduction

Indeed, traffic jams have become a significant concern over the past few decades due to the exponential growth of automobiles on the roads. As urbanization and economic development decades to progress, the number of vehicles has surged, leading to increased traffic congestion in many cities around the world. Traffic congestion has

broad effects on daily commuters and on implications for various aspects of society, including the economy, environment and public health. To address these challenges, researchers have been working on various strategies and solutions to alleviate traffic congestion and improve traffic flow. Therefore, a large number of traffic models have been proposed to explain traffic phenomena such as car-following models[1–9], continuum models[10–12] and AI models[13,14] but observations have shown that the lattice hydrodynamic model[15,16] has also been used to solve traffic problems and its variants have been useful tools in the research of traffic, as well as in the development of traffic management strategies and an understanding of traffic phenomena. Our proposed problem is based on this model and it treats traffic flow as a fluid-like phenomenon, applying principles from fluid dynamics to model the movement of vehicles on the road. To characterize the evolution of the jamming transition in traffic flow, firstly Nagatani[15] introduced lattice model.

Following that, various extensions have been carried out, taking into consideration multiple factors. These factors encompass the presence of the driver's desire[16], backward-looking and anticipation behavior[17], multi-lane situations[18], integration of the cooperative deviation[19], the predictive effect[20], driver memory effects[21], connected and non-connected vehicle behaviours[22], four-way pedestrian traffic incorporating turning capacity[23], optimal current changes with memory[24] and traffic interruption probability under honk environment[25].

The passing effect in traffic theory refers to a phenomenon in which vehicles overtake another vehicle and can create a disturbance in the traffic flow behind it. This disturbance is often characterized by a temporary reduction in the speed of surrounding vehicles and an increase in traffic density, which can lead to a ripple effect, propagate backwards through the traffic stream. Additionally, psychological headway comes into play when drivers decide how closely they want to follow the vehicle in front of them while considering the possibility of passing. In real traffic, the driver consistently adapts their velocity to match the surrounding traffic conditions while driving and relies on their instincts to determine when and how to overtake other vehicles, taking into account the psychological concept of following distance. When we mention PDS, we're addressing the preferred or perceived spacing between vehicles that drivers uphold for reasons of safety and comfort, not the quantifiable physical distance between the vehicles. In the earlier models, the traffic flow analysis is done through various factors mentioned above but lacks the information of psychological view of the individual driver, which is very important at the micro as well as macro level to overcome the issues related to traffic flow. However, to the best of the author's knowledge, no one has previously explored the lattice hydrodynamic model incorporating the factors of psychological headway and passing. Therefore, to fill this gap, we used psychological driver's view during overtaking (passing) in our study. By considering the psychological driver's sensitivity and the passing effect, the lattice hydrodynamics traffic flow model can better capture real-world traffic phenomena, including the propagation of traffic waves, the formation of congestion, and the emergence of passing maneuvers.

The paper's structure comprises four sections, each addressing distinct aspects of research on traffic flow modeling. These sections and their respective contents are detailed as follows: Section 2 introduces a refined and versatile lattice model for single-lane traffic, incorporating both the driver's psychological driver sensitivity and the passing effect. Section 3 undertakes a detailed linear, nonlinear analysis and numerical simulations of the proposed model. Section 4 provides the concluding remarks.

2 Methodology

2.1 Modelling

Nagatani[15] developed the first basic lattice hydrodynamic model with the intention of investigating the growth and propagation of "density waves" in traffic flow on a unidirectional single-lane highway. The model equation is described as

$$\rho_j(t+\tau)-\rho_j(t)+\tau\rho_0\left[\rho_j(t)v_j(t)-\rho_{j-1}(t)v_{j-1}(t)\right]=0 \tag{1}$$

$$\rho_j(t+\tau)v_j(t+\tau)=\rho_0 V\left(\rho_{j+1}\right) \tag{2}$$

Here, Equations (1) and (2) are the dynamical equations for "the conservation of mass" and "flow evolution equation". In the context of time t, $\rho_j(t)$ stands for the local density and $v_j(t)$ corresponds to the velocity at the j^{th} location on one-dimensional lattice. The average density is ρ_0 and the driver's receptiveness is quantified by $a=1/\tau$. In the above expression, the "optimal velocity function" is

$$V\left(\rho_j(t)\right)=\frac{V_{max}}{2}\left[tanh\left(\frac{1}{\rho_j}-\frac{1}{\rho_c}\right)+tanh\left(\frac{1}{\rho_c}\right)\right] \tag{3}$$

where V_{max} and ρ_c denote the maximal velocity and the safety-critical density, respectively. Later on, Nagatani extended the above model to incorporate the impact of passing by assuming that drivers attempt to overtake sluggish vehicles in order to maintain their preferred travel speed. As soon as the driver encounters congestion or reduced vehicle speeds at site- j, the vehicles attempt to pass the vehicles ahead of them and the amount of passing depends on how much the traffic volume at site- j+1 differ from that at site- j the traffic volume at the next site- j+2. On account of the passing effect, the flow evolution equation is given as

$$\rho_j(t+\tau)\nu_j(t+\tau) = \rho_0 V(\rho_{j+1}(t)) + \gamma[\rho_0 V(\rho_{j+1}(t) - \rho_0 V(\rho_{j+2}(t))] \tag{4}$$

where γ is the passing constant and V(.) is the "optimal velocity function" as discussed above. Here, we use the above equation to determine the flow at site- j, where driver is positioned. If the driver is at site- j, the driver will look ahead mainly at least two vehicles or more. If the driver encounters a large number of vehicles ahead of them, either driver can slow down their speed or attempt to pass/overtake the vehicles at site- j+1 to move on the next site- j+2 for smooth driving. To do so, the driver usually estimates the difference in the optimal flow of leading sites and accordingly, he reacts as well as takes action. Subsequently, scholars have achieved notable progress within the domain of lattice hydrodynamic models for traffic flow and introduced a range of modifications and considerations [24] to improve the model's authenticity and practicality. The importance of understanding human reactions to the environment is critical in developing road systems that prioritize safety and efficiency with the increasing number of vehicles on roads. Drivers' psychological headway (PH) [1] is considered in these modifications, providing insights into decision-making and response while driving, walking or cycling. The resulting model equation is as follows:

$$\frac{dv_n(t)}{dt} = a[V(\alpha_n \Delta x_n) - v_n(t)] + \lambda \Delta v_n(t) \tag{5}$$

Here, α_n represents the psychological response coefficient. It has been shown that a car-following model with a lower PH than an optimal velocity difference model can increase stability in situations of high traffic density. Meanwhile, heterogeneous models with higher psychological holdover can be more stable when traffic density is low.

However, there has been limited research so far on LH traffic model, specifically considering psychological factors. Individual distinctions contribute to the discrepancy between psychological and actual distances. People vary in their perceptions of the same headway, some drivers interpret it as far, while others gauge it as relatively near. In this phenomenon, the view or perspective of the driver about passing plays an important role, which is called the psychological behaviour of the driver. As we know, during passing, the driver always looks forward to headway to make the decision to pass the vehicles. In order to see the effect of psychological driver sensitivity (PDS) with passing, we modified the LH model in which the continuity equation was retained, but the flow evolution equation is altered to incorporate the influence of PDS passing and we have

$$\rho_j(t+\tau)\nu_j(t+\tau) = \rho_0 V(\alpha\rho_{j+1}(t)) + \gamma[\rho_0 V(\alpha\rho_{j+1}(t)) - \rho_0 V(\alpha\rho_{j+2}(t))] \tag{6}$$

Here $\alpha$is the psychological sensitivity coefficient in view of density. Whenever $\alpha > 1$, it means the psychological driver's sensitivity is higher than their actual sensitivity. For low density, driver becomes more confident and willing to drive more quickly. Similarly, we get the opposite response when $\alpha < 1$. The updated "optimal velocity function" is

$$V(\alpha\rho_j(t)) = \frac{V_{max}}{2tanh(\frac{1}{\alpha\rho_j}\frac{1}{\rho_c}tanh(\frac{1}{\rho_c}} \tag{7}$$

The density equation can be obtained by removing the velocity ν_j from Equations (1) and (6) and we have

$$\rho_j(t+2\tau) - \rho_j(t+\tau) + \tau\rho_0^2[V(\alpha\rho_{j+1}) - V(\alpha\rho_j)] - \gamma\tau\rho_0^2[V(\alpha\rho_{j+2}) - 2V(\alpha\rho_{j+1}) + V(\alpha\rho_j)] = 0 \tag{8}$$

when we take α = 1, then the equation reduces to the one discussed by Nagatani [15].

3 Results and Discussion

3.1 Linear Stability Analysis

The objective of this section is to perform linear stability analysis, shedding light on the impact of passing maneuvers and the psychological sensitivity of drivers on stability of traffic flow. For uniform traffic, we define the optimal velocity as $V(\alpha\rho_0)$ and the traffic density as ρ_0. Now, let's examine the stable solution for homogeneous traffic flow which is given by

$$\rho_j(t) = \rho_0 \tag{9}$$

$$V(\alpha\rho_j(t)) = V(\alpha\rho_0) \tag{10}$$

Assume that the steady-state density of site-j is perturbed slightly by $\eta_j(t)$. Then

$$\rho_j(t) = \rho_0 + \eta_j(t) \tag{11}$$

$$V(\alpha\rho_j(t)) = V(\alpha\rho_0) + V'(\alpha\rho_0)\alpha\eta_j(t) \tag{12}$$

Using Equation (11) in Equation (8), we get

$$\eta_j(t+2\tau) - \eta_j(t+\tau) + \tau\rho_0^2 V'(\alpha\rho_0)[\eta_{j+1} - \eta_j] - \gamma\tau\rho_0^2 V'(\alpha\rho_0)[\eta_j - 2\eta_{j+1} + \eta_{j+2}] = 0 \tag{13}$$

where $V'(\alpha\rho_0(t)) = \frac{dV(\alpha\rho)}{d\rho}$ at $\rho = \rho_0$.

Using the expression $\eta_j(t) = e^{ikj+zt}$ in Equation (13), we get

$$e^{2zt} - e^{zt} + \alpha\tau\rho_0^2 V'(\alpha\rho_0)[e^{ik} - 1] - \tau\gamma\rho_0^2 V'(\alpha\rho_0)[1 - 2e^{ik} + e^{2ik}] = 0 \tag{14}$$

By taking $z = z_1(ik) + z_2(ik)^2 + \ldots$into Equation (14), we obtain

$$\begin{aligned} &2\tau z_1(ik) - 2\tau z_2(ik)^2 - \frac{\tau^2}{2}[z_1^2(ik)^2] + 2\tau^2 z_1^2(ik)^2 - \tau z_1(ik) - \tau z_2(ik)^2 + \tau\rho_0^2\alpha V^{'}(\alpha\rho_0)(ik) \\ &+\tau\rho_0^2\alpha V^{'}(\alpha\rho_0)(\frac{(ik)^2}{2}) - \gamma\tau\rho_0^2\alpha V^{'}(\alpha\rho_0)(ik)^2 = 0 \end{aligned} \tag{15}$$

We have calculated the coefficient of first and second-order terms of ik and $(ik)^2$, respectively as

$$z_1 = -\rho_0^2\alpha V'(\alpha\rho_0) \tag{16}$$

$$z_2 = \frac{3}{2}\tau(\rho_0^2 V'(\alpha\rho_0))^2 - \frac{1-2\gamma}{2}(\rho_0^2 V'(\alpha\rho_0) \tag{17}$$

Long-wavelength waves cause the "uniform steady-state flow" to become "unstable" when $z_2 < 0$ and become stable as long as $z_2 > 0$. As a result, the "neutral stability curve" is represented by

$$\tau = \frac{1-2\gamma}{3\rho_0^2\alpha V'(\alpha\rho_0)} \tag{18}$$

It is evident from Equation (18) that the parameters α and γ actively contribute to stabilize traffic flow, ensuring a steady flow profile for a comfortable experience.

The phase diagrams in density-sensitivity for the basic model and proposed model are compared in Figure 1. On comparison, it becomes clear that the latter displays a more stable zone for this specific value of $\alpha = 0.9$. This indicates that the proposed model represents a refinement of existing work. It emphasises the value of psychological driver's sensitivity as well as passing and how it affects maintaining a reliable and secure traffic flow.

Figure 2 shows the neutral stability curves in density-sensitivity space and the apex of each curve indicates the critical point for different values of α when the passing rate is different. The stable region lies above the neutral curves, where traffic jams are not observed, while the unstable region lies below the neutral curves, where density waves are observed.

Figure 2 clearly illustrates that the amplitude of these curves grows with the increase in the values of γ for α = 0.9. This suggests that higher values of γ lead to the expansion of an unstable region. Figure 2, also shows that as γ goes up, so does the amplitude of the stability curve for α = 1.1 to 1.2. This implies that higher values of γ contribute to the enlargement of an unstable region. The neutral stability curves increase along with the psychological sensitivity coefficient α, but the critical points get decreased. In addition to this, it is also noted that the value of critical density, which is the point of inflexion of the

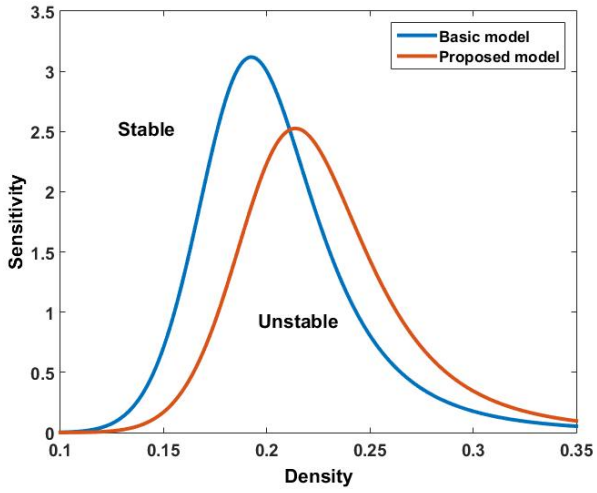

Fig 1. Comparative diagram in density-sensitivity forbasic and p roposed model with $\alpha = 0.9$ and $\gamma = 0$

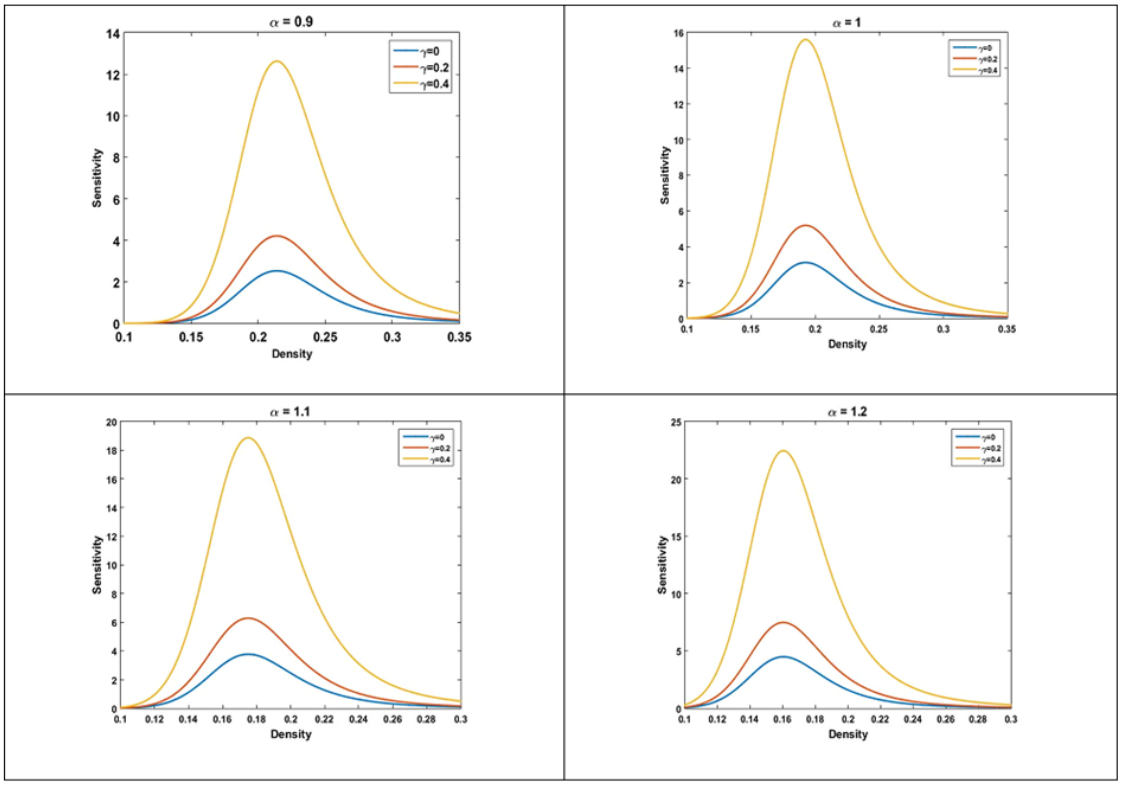

Fig 2. Phase diagram in density-sensitivity for different value of γ with fix α

neutral stability curve, decreases with growth in the value of α. However, the stable region is decreasing for lower values of γ at low density while it enhances at a higher value of density.

By comparing different part of Figure 2, we noticed that the amount of traffic congestion is reducing with decreases in the value of psychological sensitivity because drivers estimate that the psychological headway is smaller than the actual headway and try to overtake the leading vehicles. On the other hand, if the driver thinks that he needs more space to overtake as compared to actual headway, it may lead to congestion which is clear from the patterns of Figure 2 for α = 1 and α = 1.1.

Therefore, we can draw the conclusion that decreasing psychological driver sensitivity can enhance stability in high-traffic conditions, whereas utilizing model featuring a larger psychological driver sensitivity yields greater instability in situations of low traffic density. Therefore, by altering psychological and passing values, one can understand the psychological view of drivers in the study of the transportation system and its application in reducing traffic congestion.

3.2 Nonlinear

To investigate the nonlinear behavior near the critical point, we used the slower variables X and T. Nonlinear analysis allows for the examination of complex interactions between variables that may not be evident in a linear analysis. It can reveal emergent behaviors, stability, instability, and other intricate characteristics that are not apparent in simpler linear analysis. The analysis is focused on a coarse scale, which means they looked at large-scale patterns in the traffic flow. For a small positive parameter ε, the slow variables X and T are defined as

$$X = \varepsilon(j + bt), T = \varepsilon^3 t \tag{19}$$

where b is constant to be determined. Let $\rho_j$satisfy the following equation:

$$\rho_j(t) = \rho_c + \varepsilon R(X,T) \tag{20}$$

The following nonlinear partial differential equation is obtained by using Equations (19) and (20) to expand Equation (8) up to the fifth order of ε:

$$\begin{aligned}&\varepsilon^2\kappa_1\partial_X R + \varepsilon^3\kappa_2\partial_X^2 R + \varepsilon^4(\partial_T R + \kappa_3\partial_X^3 R + \kappa_4\partial_X R^3)\\&+\varepsilon^5(\kappa_5\partial_T\partial_X R + \kappa_6\partial_X^4 R + \kappa_7\partial_X^2 R^3) = 0\end{aligned} \tag{21}$$

where the coefficients $\kappa_i (i = 1, 2..., 7)$ are

$\kappa_1 = b + \alpha\rho_c^2 V'(\alpha\rho_c)$,
$\kappa_2 = \frac{3}{2}b^2\tau^2 + \frac{\tau\alpha\rho_c^2 V'(\alpha\rho_c)}{2} - \gamma\alpha\rho_c^2 V'(\alpha\rho_c)$,
$\kappa_3 = \frac{7}{6}b^3\tau^3 + \frac{\tau\alpha\rho_c^2 V'(\alpha\rho_c)}{6} - \gamma\alpha\rho_c^2 V'(\alpha\rho_c)$,
$\kappa_4 = \frac{\tau\alpha^3\rho_c^2 V'''(\alpha\rho_c)}{6}$,
$\kappa_5 = 3b\tau^2$,
$\kappa_6 = \frac{15}{24}b^4\tau^4 + \frac{\tau\alpha\rho_c^2 V'(\alpha\rho_c)}{24} - 14\frac{\gamma\tau\alpha\rho_c^2 V'(\alpha\rho_c)}{24}$,
$\kappa_7 = \frac{\tau\alpha^3\rho_c^2 V'''(\alpha\rho_c)}{12} - \gamma\frac{\tau\alpha^3\rho_c^2 V'''(\alpha\rho_c)}{6}$.
where $V' = \frac{dV(\rho)}{d\rho}$ and $V''' = \frac{d^3V(\alpha\rho)}{d\rho^3}$ at $\rho = \rho_c$.

In the neighborhood of critical point τ_c, we define $\tau = \tau_c(1 + \varepsilon^2)$ and choosing $b = -\alpha\rho_c^2 V'(\alpha\rho_c)$, we get

$$\varepsilon^4(\partial_T R + \mu_1\partial_X^3 R + \mu_2\partial_X R^3) + \varepsilon^5(\mu_3\partial_X^2 R + \mu_4\partial_X^4 R + \mu_5\partial_X^2 R^3) = 0 \tag{22}$$

where the coefficients $\mu_i (i = 1, 2, 3, 4, 5)$ are

$\mu_1 = -\alpha\rho_c^2 V'(\alpha\rho_c)(-\frac{7}{54}(1-2\gamma)^2 + \frac{1}{6} - \gamma)$,
$\mu_2 = \frac{\alpha^3\rho_c^2 V'''(\alpha\rho_c)}{6}$,
$\mu_3 = -\tau\alpha\rho_c^2 V'(\alpha\rho_c)(\frac{1-2\gamma}{2})$,
$\mu_4 = \alpha\rho_c^2 V'(\alpha\rho_c)[\frac{1}{24}(\frac{58}{9})(1-2\gamma)^3 + \frac{1}{24}(1-14\gamma) + (\gamma - \frac{1}{6})(1-2\gamma)]$,
$\mu_5 = -\frac{\tau\alpha^3\rho_c^2 V'''(\alpha\rho_c)}{6}(\frac{1-2\gamma}{2})$.

In order to derive the standard mKdV equation, we perform the following transformations in Equation (22):

$T' = \mu_1 T, R = \sqrt{\frac{\mu_1}{\mu_2}}R'$

After implementing the transformation in Equation (22), we obtain

$$\partial_T R' - \partial_X^3 R' + \partial_X R'^3 + \varepsilon \bar{M}[R'] = 0, \tag{23}$$

where $\bar{M}[R'] = \frac{1}{\mu_1}(\mu_3 \partial_X^2 R' + \frac{\mu_1 \mu_5}{\mu_2} \partial_X^2 R'^3 + \mu_4 \partial_X^4 R')$

We obtain the usual mKdV equation after neglecting the (ϵ) terms in Equation (23) and intended kink-soliton solution is given by

$$R_0^{'}(X,T') = \sqrt{c} tanh \sqrt{\frac{c}{2}(X - cT')} \tag{24}$$

The solvability condition must be met in order to calculate the propagation velocity for the kink-antikink solution

$$(R_0^{'} \overline{M}[R_0^{'}]) = \int_{-\infty}^{\infty} dX R_0^{'} \overline{M}[R_0^{'}] = 0 \tag{25}$$

with $\bar{M}[R_0^{'}] = \bar{M}[R']$.

By solving Equation (25), the value of c is

$$c = \frac{5\mu_2 \mu_5}{2\mu_2 \mu_4 - 3\mu_1 \mu_5}. \tag{26}$$

Hence, the "kink-antikink" solution is given by

$$\rho_j(t) = \rho_c + \varepsilon \sqrt{\frac{\mu_1 c}{\mu_2}} tanh \sqrt{\frac{c}{2}(X - c\mu_1 T)}, \tag{27}$$

with $\varepsilon^2 = \frac{\tau}{\tau_c} - 1$ and the amplitude A of the solution is

$$A = \sqrt{\frac{\mu_1}{\mu_2} \varepsilon^2 c}. \tag{28}$$

Two coexisting phases can be understood by the "kink-antikink" soliton solution. There is a congested high density phase as well as a low-density phase that is free to move, which may be separated from one another using the equation $\rho_j = \rho_c \pm A$ in the phase space (ρ, a).

3.3 Simulation

We used "numerical simulation" to validate the theoretical findings of the proposed model with the influence of the psychological driver's sensitivity and passing effect. Periodic boundary conditions are established in order to explicitly replicate traffic behaviour and the initial conditions are

$$\rho_j(0) = \rho_j(1) = \begin{cases} \rho_0 - A \, if \, 0 \leq j < \frac{M}{2} \\ \rho_0 - A \, if \, \frac{M}{2} \leq j < M \end{cases}$$

where A is the initial disturbance and M = 100 is the total number of sites, the relevant parameters are $\rho_0 = \rho_c = 0.2$, V_{max} and A = 0.005.

Figures 3, 4, 5 and 6 offer a clear depiction of the spatiotemporal evolution of density, specifically between time t=20000—20300. For the values α =0.9 and a =2.6, stable region is reached, the perturbation at the beginning dies out over time, and the flow becomes uniform as shown in Figure 3 (part first). In pattern (part second) and pattern (part third), a further increase in γ from 0 to 0.4 illustrates that the perturbation creates stop-and-go traffic that travels the other way. It's amplified with an increase in the value of γ (part second and third), which increases the amplitude of these kink-antikink density waves. When α =1 and a =3.2, as the stability is satisfied, the spatiotemporal evolution of density has become uniform for γ = 0 while it becomes fluctuation for γ = 0.2 and 0.4 as shown in patterns (part second) and (part third) of Figure 4 respectively. Furthermore, these fluctuations get amplified with increasing passing rates. To check the effect of advanced psychological driver's sensitivity on traffic flow, we also analyzed the results for α =1.1 and 1.2; the graphical representations for these are shown in Figures 5 and 6, respectively. For a =1.3 and a =2.8, initially, when γ = 0, we reach into the stable zone, so the fluctuation does not appear,

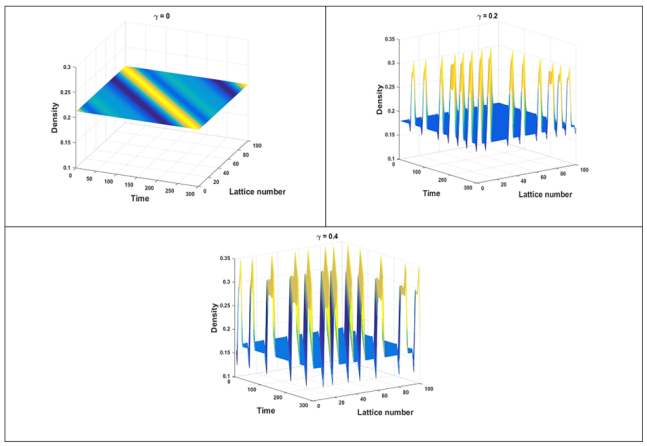

Fig 3. Spatiotemporal evolutions of density at time t=20300 for a =2.6, α = 0.9 with different γ

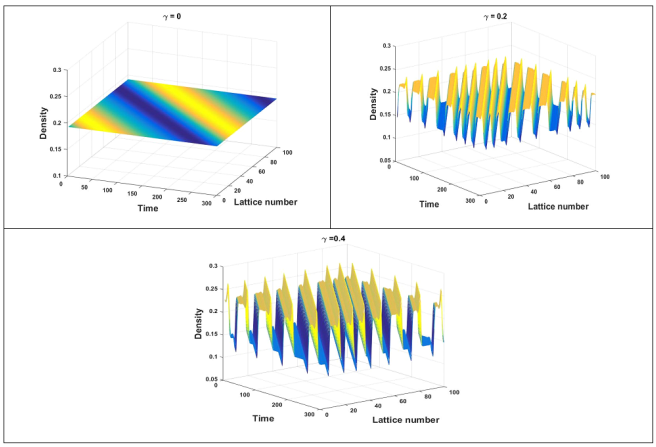

Fig 4. Spatiotemporal evolutions of density at time t=20300 for a =3.2, α = 1 with different γ

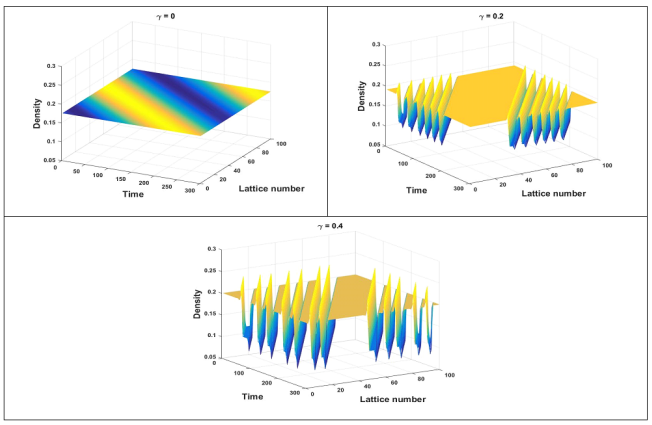

Fig 5. Spatiotemporal evolutions of density at time t=20300 for a =2.8, α = 1.1 with different γ

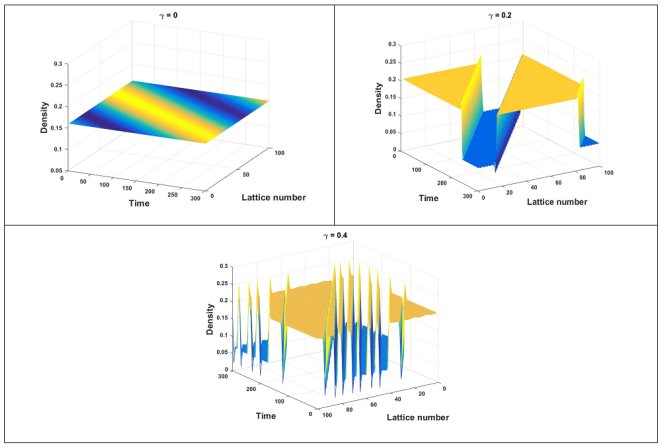

Fig 6. Spatiotemporal evolutions of density at time t=20300 when a = 1.3 and α = 1.2 with different γ

and congestion does not appear as shown in Figure 5 (part first) and Figure 6 (part first). But as the value of the passing increases, we enter into the unstable region and therefore the congestion appears in the form of kink-antkink density waves, which are the solution of the mKdV equation.

In Figure 7, we observe the changes in density as time progresses beyond t = 20,300s for γ = 0.0, 0.2, 0.4 for different values of α. On Looking towards the Figure 7 (part first) that is plotted for α = 0.9 and a = 2.6 for different values of γ, it is obvious that for lower values of γ, the perturbation which is added to the initial flow of traffic dies out after a long time and traffic flow becomes uniform for γ = 0. As the value of γ increases from 0.2 to 0.4, a small perturbation is converted into stop-and-go traffic waves and these observations are the same as those that happen in real traffic that travels in the reverse direction. A similar kind of phenomenon is happening for all values of psychological driver sensitivity, as shown in patterns (part second), (part third) and (part fourth) of Figure 7. These density profiles show distinct travelling waves with varying speeds, which are separated by a growing and decaying density region. The number of stop-and-go waves decreases with an increase in the coefficients of psychological driver sensitivity in overtaking, which means that the psychological sensitivity enhances the stability of the traffic flow.

It can be observed that an increase in the value of α corresponds to better stability of traffic flow. It is clear from Figure 7 (part first to fourth) that the integration of passing constants for fixed PDS plays a significant role in alleviating traffic jams, thus providing empirical validation for the theoretical findings. The amplitude of density waves is weakened with the decrease in the coefficient of psychological sensitivity and passing. The lack of fulfillment of the stability condition leads to the evolution of initial disturbances into a congested flow. Due to the unsatisfied stability condition, the initial disturbances transform into a congested flow.

Moreover, the study shows that when the coefficient of passing is equal to zero, the traffic jam completely disappears, and the flow of traffic becomes uniform. This finding emphasizes the importance of implementing efficient traffic control strategies that consider the impact of PDS on traffic flow stability. Overall, Figure 7 provide valuable insights into the dynamics of traffic flow and how it can be stabilized through PDS measures. Thus, these simulations underscore the importance of PDS and passing effect in influencing traffic stability. It is observed that a larger PDS does not effectively alleviate traffic congestion when traffic density is high. However, under low traffic density, a larger PDS improves traffic stability and increases traffic flux.

To effectively distinguish traffic situations, "density differences" are plotted in phase space $\rho_j(t)$ against $\rho_j(t)-\rho_j(t-1)$ at time t=20300s for different values of γ, in Figure 8 correspond to the patterns in Figure 7 between time t=20000–20300s. The configuration depicted in Figure 8 corresponds to a set of dispersed points within the phase space plot. When α is set to lower values, the pattern assumes a limit cycle, resembling the scenario presented in Figure 8 (part first to third), indicating periodic traffic behavior. With increasing α, the pattern shifts to exhibit scattered plots surrounding a closed loop, representing irregular traffic patterns. This chaotic behavior reflects the distinct characteristics associated with chaos, where the points on the right and left ends represent states of traffic congestion and smoothly flowing traffic, respectively.

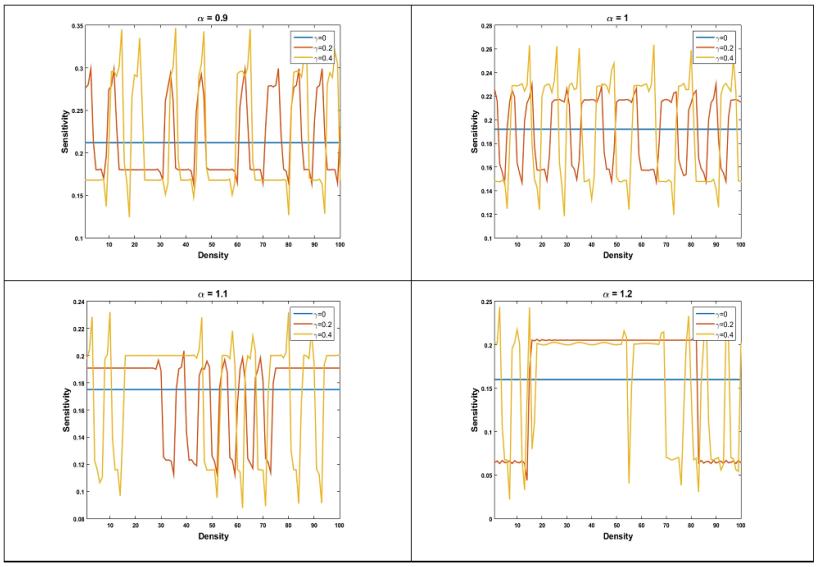

Fig 7. Density profiles at time t=20300s for different values of γ with fix α

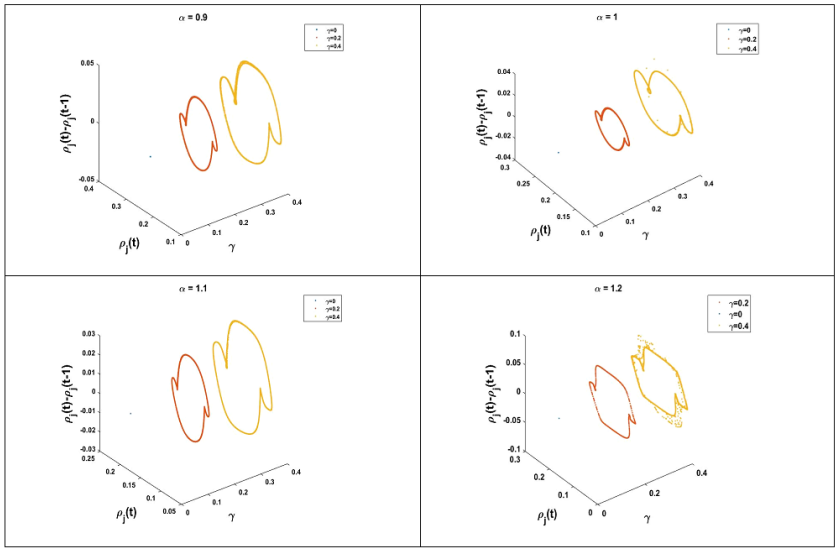

Fig 8. Plot of density difference $\rho_j(t)$ against $\rho_j(t) - \rho_j(t-1)$ at time t=20300s for different values of γ with fix α

4 Conclusion

In this study, we investigated the effect of psychological driver's sensitivity (PDS) with a passing effect in a new lattice model. After combining these factors, the traffic flow becomes more efficient, safe, and stable and gives better performance to existing models which clearly seen from our findings. The influence of psychological factor with passing is investigated using linear stability analysis. Nonlinear stability analysis revealed the range of PDS with a passing constant for which the kink soliton solution exists. For lesser values of the coefficient of PDS and passing effect, the phase diagram shows traffic flow becomes more stable. By incorporating the PDS with passing into the proposed lattice model, the theoretical conclusions are validated through numerical simulation, demonstrating the effectiveness of the proposed approach in alleviating traffic bottlenecks.

Acknowledgements

Meenakshi Mehra gratefully acknowledge financial support from the "University Grant Commission (UGC), New Delhi, India", under file no. F.16-6(DEC.2018)/2019.

Data Availability Statement

There are no data related to this manuscript.

References

1) Wang J, Sun F, Cheng R, Ge H. An extended heterogeneous car-following model with the consideration of the drivers' different psychological headways. *Physica A: Statistical Mechanics and its Applications*. 2018;506:1113–1125. Available from: https://doi.org/10.1016/j.physa.2018.05.040.
2) Yadav S, Redhu P. Driver's attention effect in car-following model with passing under V2V environment. *Nonlinear Dynamics*. 2023;111:13245–13261. Available from: https://doi.org/10.1007/s11071-023-08548-x.
3) Yadav S, Siwach V, Redhu P. Impact of driver's advanced reaction time in car-following model with optimal velocity deviation under V2X environment. *Europhysics Letters*. 2023;143(5). Available from: https://doi.org/10.1209/0295-5075/acf51d.
4) Peng GH. A new car-following model with driver's anticipation effect of traffic interruption probability. *Chinese Physics B*. 2020;29(8). Available from: https://iopscience.iop.org/article/10.1088/1674-1056/ab9293/pdf.
5) Peng GH, Tang R, Kuang H, Tan HL, Chen T. CO2 emission control in new CM car-following model with feedback control of the optimal estimation of velocity difference under V2X environment. *Chinese Physics B*. 2021;30(10). Available from: https://iopscience.iop.org/article/10.1088/1674-1056/ac1417.
6) Zhai C, Wu W, Xiao Y. Cooperative car-following control with electronic throttle and perceived headway errors on gyroidal roads. *Applied Mathematical Modelling*. 2022;108:770–786. Available from: https://doi.org/10.1016/j.apm.2022.04.010.
7) Redhu P, Sunita, Meenkashi. Driver Predictions and Energy Consumption in Car-following Model with BFL Effect. *Communications in Mathematics and Applications*. 2023;14(2):727–744. Available from: https://doi.org/10.26713/cma.v14i2.2169.
8) Yadav S, Redhu P. Bifurcation Analysis of Driver's Characteristics in Car-Following Model. *Journal of Computational and Nonlinear Dynamics*. 2023;18(11):1–9. Available from: https://doi.org/10.1115/1.4063338.
9) Yadav S, Redhu P. Impact of driving prediction on headway and velocity in car-following model under V2X environment. *Physica A: Statistical Mechanics and its Applications*. 2024;635. Available from: https://doi.org/10.1016/j.physa.2024.129493.
10) Zhai C, Wu W, Xiao Y. Non-lane-discipline-based continuum model considering the effect of lateral gaps and electronic throttle dynamics. *Chinese Journal of Physics*. 2023;83:253–269. Available from: https://doi.org/10.1016/j.cjph.2023.03.013.
11) Yu L. A new continuum traffic flow model with two delays. *Physica A: Statistical Mechanics and its Applications*. 2020;545. Available from: https://doi.org/10.1016/j.physa.2019.123757.
12) Hadadi F, Tehrani HG, Aghayan I. An extended non-lane-discipline-based continuum model through driver behaviors for analyzing multi-traffic flows. *Physica A: Statistical Mechanics and its Applications*. 2023;625. Available from: https://doi.org/10.1016/j.physa.2023.128965.
13) Naheliya B, Redhu P, Kumar K. MFOA-Bi-LSTM: An optimized bidirectional long short-term memory model for short-term traffic flow prediction. *Physica A: Statistical Mechanics and its Applications*. 2024;634. Available from: https://doi.org/10.1016/j.physa.2023.129448.
14) Naheliya B, Redhu P, Kumar K. A Hybrid Deep Learning Method for Short-Term Traffic Flow Forecasting: GSA-LSTM. *Indian Journal of Science and Technology*. 2023;16(46):4358–4368. Available from: https://doi.org/10.17485/IJST/v16i46.2520.
15) Nagatani T. Modified KdV equation for jamming transition in the continuum models of traffic. *Physica A Statistical Mechanics and its Applications*. 1998;261(3-4):599–607. Available from: https://doi.org/10.1016/S0378-4371(98)00347-1.
16) Wang J, Sun F, Ge H. An improved lattice hydrodynamic model considering the driver's desire of driving smoothly. *Physica A: Statistical Mechanics and its Applications*. 2019;515:119–129. Available from: https://doi.org/10.1016/j.physa.2018.09.155.
17) Wan J, Huang X, Qin W, Gu X, Zhao M. An Improved Lattice Hydrodynamic Model by considering the Effect of "Backward-Looking" and Anticipation Behavior. *Complexity*. 2021;2021:1–12. Available from: https://doi.org/10.1155/2021/4642202.
18) Madaan N, Sharma S. A lattice model accounting for multi-lane traffic system. *Physica A: Statistical Mechanics and its Applications*. 2021;564. Available from: https://doi.org/10.1016/j.physa.2020.125446.
19) Peng GH, Luo CL, Zhao HZ, Tan HL. A novel lattice model integrating the cooperative deviation of density and optimal flux under V2X environment. *Chinese Physics B*. 2023;32(1). Available from: https://iopscience.iop.org/article/10.1088/1674-1056/ac65f1/meta.
20) Liu H, Cheng R, Xu T. Analysis of a Novel Two-Dimensional Lattice Hydrodynamic Model Considering Predictive Effect. *Mathematics*. 2021;9(19):1–13. Available from: https://dx.doi.org/10.3390/math9192464.
21) Li L, Cheng R, Ge H. New feedback control for a novel two-dimensional lattice hydrodynamic model considering driver's memory effect. *Physica A: Statistical Mechanics and its Applications*. 2021;561. Available from: https://dx.doi.org/10.1016/j.physa.2020.125295.
22) Zhang Y, Zhao M, Sun D, Wang SH, Huang S, Chen D. Analysis of mixed traffic with connected and non-connected vehicles based on lattice hydrodynamic model. *Communications in Nonlinear Science and Numerical Simulation*. 2021;94. Available from: https://doi.org/10.1016/j.cnsns.2020.105541.
23) Tang Y, Xue Y, Huang M, Wen Q, Cen B, Chen D. A Lattice Hydrodynamic Model for Four-Way Pedestrian Traffic with Turning Capacity. *Sustainability*. 2023;15(3):1–17. Available from: https://dx.doi.org/10.3390/su15032544.
24) Zhai C, Wu W. An extended multi-phase lattice model with consideration of optimal current changes with memory. *Cluster Computing*. 2019;22(S3):7447–7457. Available from: https://dx.doi.org/10.1007/s10586-018-1773-3.
25) Wang Q, Ge H, Cheng R. A New Two-Lane Lattice Hydrodynamic Model considering the Traffic Interruption Probability under Honk Environment. *Complexity*. 2020;2020:1–12. Available from: https://dx.doi.org/10.1155/2020/1737318.